Q. J. R. Meteorol. Soc. (2000), **126**, pp. 213–239

Influence of the Indian summer monsoon on ENSO

By BEN P. KIRTMAN* and J. SHUKLA
Center for Ocean–Land–Atmosphere Studies, USA

(Received 8 July 1998; revised 22 February 1999)

SUMMARY

Historical records (approximately 100 years) of Indian summer monsoon rainfall and El Niño/Southern Oscillation (ENSO) indices show a strong negative correlation. This negative correlation is strongest for east Pacific sea surface temperature anomalies (SSTA) that occur during the months of December through to March, which is about three to six months immediately following the monsoon season (June to September). Based on this correlation, one is tempted to speculate that monsoon variability affects ENSO variability. However, it is well known that ENSO is phase locked to the annual cycle in that the largest SSTA occur at the end of the calendar year. In other words, an ENSO which originated well before the summer monsoon season will have its peak amplitude at the end of the calendar year. The purpose of this study is to explain the impact of the monsoon which has a strong seasonal preference on ENSO which has a life cycle of about 4 years.

First, a 50-year atmospheric general-circulation model simulation with climatological SST is examined to determine the tropical Pacific wind-stress anomalies that are associated with a variable monsoon but that are also independent of SST variability in the tropical Pacific. Using simple statistical techniques, it is found that a weak (strong) monsoon results in a weakening (strengthening) of the trade winds over the tropical Pacific. To examine how these 'monsoon-forced wind-stress anomalies' in the tropical Pacific affect ENSO, simulations were made with a simple coupled model that does not include the effects of a variable monsoon. The effects of the monsoon are then added in the coupled model by either specifying the strength of the monsoon or by parametrizing the strength of the monsoon in terms of the coupled-model simulated SSTA in the east Pacific. Based on these coupled simulations, a variable monsoon enhances the ENSO variability, particularly three to six months after the monsoon ends, and can also serve as a trigger mechanism for ENSO. It is found that an ongoing warm (cold) ENSO event is made even warmer (colder) by a weak (strong) monsoon. Similarly, warm (cold) events are weakened by a strong (weak) monsoon. These results also reproduce the observed lag/lead ENSO–monsoon relation where the maximum negative correlation between the monsoon and the SSTA in the east Pacific occurs 3–6 months after the monsoon season.

KEYWORDS: El Niño Monsoon Wind stress

1. INTRODUCTION

For some time it has been recognized that the potential predictability of low-frequency atmospheric variability is due to the influence of the slowly varying boundary conditions at the earth's surface (Shukla 1984). There have been a number of studies, for example, identifying the influence of sea surface temperature (SST; Sikka 1980; Rasmusson and Carpenter 1983; Mooley and Parthasarthy 1983), soil moisture (Bavadekar and Mooley 1981; Shukla and Mintz 1982) and snow cover (Hahn and Shukla 1976; Vernekar *et al.* 1995; Bamzai and Shukla 1999), on the variability of the Indian summer monsoon. Much of the potential predictability of the monsoon and other atmospheric low-frequency variability in general, comes from the ability to predict these low-frequency variations in the surface boundary conditions. The climate system, however, is coupled. This means that low-frequency variability in the atmosphere is not only influenced by, but also influences, the low-frequency boundary conditions. The success of climate prediction, therefore, depends on understanding how low-frequency variability in the atmosphere interacts with, and affects, the boundary conditions.

Historically, however, the monsoon has been viewed as a passive element of the climate system. In other words, the circulation and rainfall anomalies associated with the variable monsoon were not thought to produce any significant impact on these slowly evolving boundary conditions and, therefore, had little influence on the potential predictability of the climate system. While it is now recognized that the monsoon is

* Corresponding author: Center for Ocean–Land–Atmosphere Studies, Institute of Global Environment and Society, Inc., 4041 Powder Mill Road, Suite 302, Calverton, MD 20705, USA. e-mail: kirtman@cola.iges.org

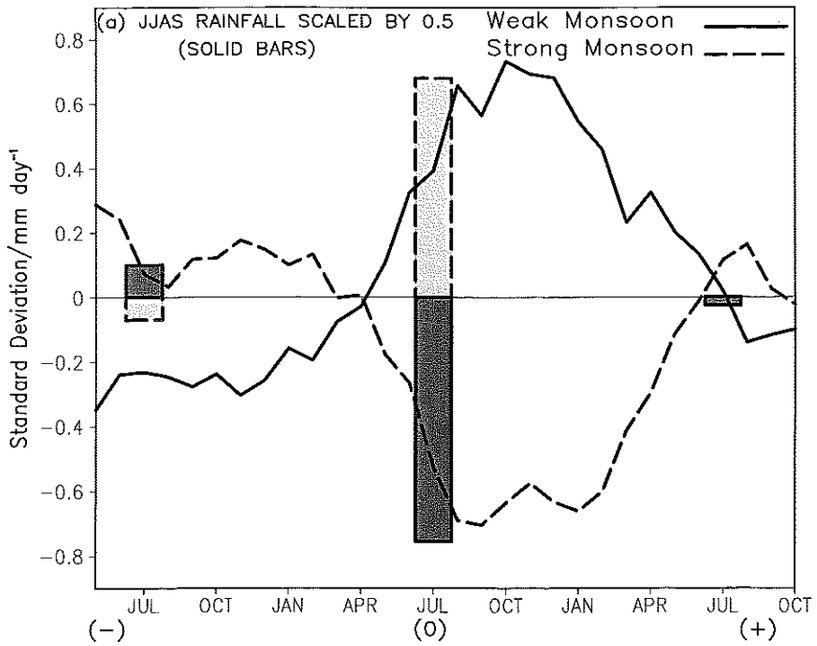

Figure 1(a). Composite time series of monthly mean sea surface temperature anomaly (SSTA) over the NINO3 region for a 30-month period (solid lines) and composite Indian summer monsoon rainfall anomaly (bars). The rainfall composites (in mm day^{-1}) are calculated based on plus (light shading) or minus (dark shading) one standard deviation. The SSTA composites are based on the rainfall composite. If the June to September (JJAS) rainfall anomaly is greater than one standard deviation away from normal, then the SSTA starting from the June of the year before (−) the monsoon to the October of the year following (+) the monsoon contributes to the composite. (Figure courtesy of M. Fennessy.)

an interactive component of the climate system that can impact the slowly evolving boundary conditions (Webster *et al.* 1998), this interaction is not well understood. In particular, it is not known how the Indian summer monsoon influences the El Niño/Southern Oscillation (ENSO) variability. The objective of the work presented here is to examine how monsoon variability affects ENSO variability.

Throughout the remainder of this paper the focus is on the variability of the Indian summer monsoon as opposed to the broader Asian–Australian monsoon system. We recognize that there are many other components of the monsoon system (e.g. the winter monsoon, the Chinese monsoon, the Australian monsoon, cold surges, intra-seasonal variability) and that these other components may also affect ENSO variability. Nevertheless, the Indian summer monsoon is a pronounced feature of the Asian–Australian monsoon system, and thus its variability can be thought of as an indicator of the variability of the broader Asian–Australian monsoon system. When we refer to 'the monsoon' we specifically mean the Indian summer monsoon.

The impact of ENSO on the Indian summer monsoon, as opposed to the impact of the monsoon on ENSO, has a rich research history, particularly from an observational perspective (e.g. Walker 1924; Bjerknes 1969). While there is considerable observational evidence that ENSO affects the monsoon (Sikka 1980; Rasmusson and Carpenter 1983; Yasunari 1990; Webster and Yang 1992; Goswami *et al.* 1999 among others),

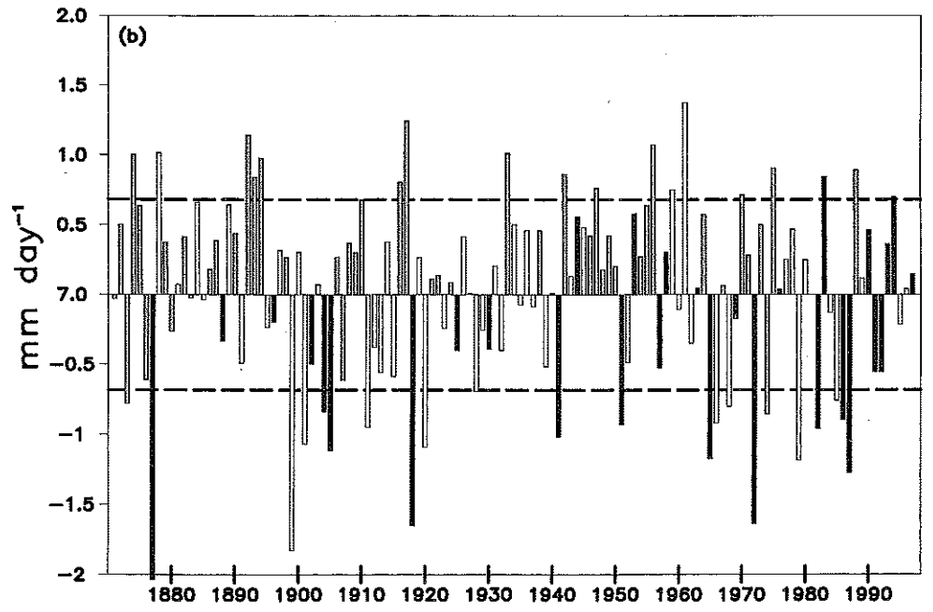

Figure 1(b). Time series of Indian summer monsoon rainfall for 1871–1997. The vertical bars are colour coded so that years with warm (greater than 0.5 standard deviation) SSTA in the east Pacific (170°W–70°W, 20°S–20°N) are dark grey and cold years (less than −0.5 standard deviation) are light shaded. The mean monsoon rainfall is 7 mm day^{-1}. (Figure courtesy of M. Fennessy.)

a clear dynamic link has not been well established (Nigam 1994). In fact, general-circulation model integrations with observed SST during the past 20 years have not been very successful in simulating the flood and drought years (Sperber and Palmer 1996).

Detailed analysis of the lag–lead relationship between the monsoon and ENSO indices (e.g. southern oscillation index or area averaged SST anomaly (SSTA) in the central and eastern Pacific) suggests a complex interaction between the monsoon and ENSO. Figure 1(a), for example, shows a composite time series of the monthly mean SSTA over the NINO3 region (5°S–5°N, 150°W–90°W) for a 30-month period; the bars denote the Indian monsoon composite rainfall anomaly. The rainfall data were provided by Parthasarthy *et al.* (1993) and the SST data are from the Hadley Centre global sea ice and SST dataset (GISST2.2a, Parker *et al.* 1995). The SSTA composites are based on Indian monsoon rainfall anomalies for 1901–75. If, for example, the all-Indian rainfall was greater than one standard deviation away from normal from June through to September 1918, then the SSTA from July 1917 to October 1919 was averaged into the composite. It is clearly seen that the largest SSTA occurs three to six months after the monsoon season. It is also clear that the SSTA associated with these warm ENSO events started much earlier in the year, well before the monsoon season. It is well known (Zebiak and Cane 1987) that the initiation and evolution of ENSO giving rise to a maximum SSTA during the end of the calendar year can occur simply by coupled ocean–atmosphere interactions in the tropical Pacific basin only. Therefore, it is not clear, just by this composite analysis, if the monsoon anomalies have any role in influencing the evolution of the ENSO SSTA.

The consistency of the contemporaneous relationship between the monsoon and ENSO can be detected in Fig. 1(b). Figure 1(b) shows the all-India standardized

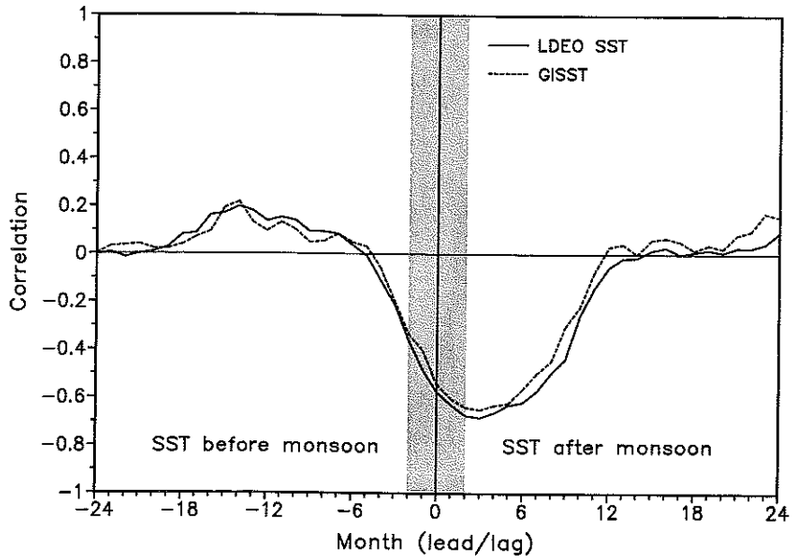

Figure 2. Lag/lead correlation between all-India June–September rainfall anomalies and NINO3 sea surface temperature anomaly. (Figure courtesy of V. Krishnamurthy.) Two datasets were used (see text). The shading denotes the boundaries of the monsoon season.

monsoon rainfall anomaly from 1871 to 1997. During a large fraction of the flood (drought) years, the contemporaneous SSTA in the east Pacific is relatively cold (warm). In parametrizing the effects of the monsoon, we will be using this contemporaneous relationship. On the other hand, the relationship between the monsoon and ENSO is not perfect. By this we mean that there are years with strong monsoon rainfall anomalies where there is no substantial SSTA in the east Pacific. Similarly, there are flood (drought) years where there is either no substantial ENSO anomaly or the east Pacific is warmer (colder) than normal.

Figure 2 shows the NINO3 averaged SSTA correlated with all-India summer monsoon precipitation anomalies. Two different SSTA datasets were used (Parker *et al.* 1995; Kaplan *et al.* 1997) to calculate the lag–lead correlation. The NINO3 SSTAs well before the monsoon (at least six months) have a weak positive correlation with all-Indian monsoon rainfall anomalies. Starting with the SSTA leading the monsoon by six months, the correlations rapidly become negative with a contemporaneous correlation of approximately −0.6. Similar to the composite analysis, the strongest negative correlations occur three to six months after the monsoon.

While the composite analysis and the correlations do not necessarily imply a cause and effect relationship, they have led to the suggestion that Indian summer monsoon anomalies can trigger ENSO events (Barnett *et al.* 1991; Yasunari and Seki 1992). Barnett *et al.* (1991), for example, argue that the amount and extent of Asian snow cover has a subsequent effect on the Asian monsoon, and the resulting monsoon perturbation may in turn trigger ENSO events. Yasunari and Seki (1992) describe a monsoon and coupled ocean–atmosphere system where the interaction of this system and the North Atlantic oscillation leads to the irregularity of ENSO through stochastic forcing. Nigam (1994) used a linear model forced by heating anomalies in the greater monsoon region to diagnose the impact of an anomalous monsoon on global near-surface wind anomalies. Although very weak, he found that the wind anomalies in the Pacific were

consistent with the observed ENSO–monsoon relationship (i.e. weak monsoon—weak trade winds).

In addition to the Barnett *et al.* (1991) study, there have been some attempts to examine how a variable monsoon affects ENSO in coupled models. Wainer and Webster (1996) prescribed idealized monsoon forcing in a simple coupled model and argued that a variable monsoon could explain the irregularity of ENSO. Chung and Nigam (1999, hereafter CN) also empirically incorporated anomalous monsoon heating into a simple coupled model but, distinct from the Wainer and Webster study, the monsoon was an interactive component of the coupled model that enhanced the ENSO activity.

The primary difficulty in understanding how the Indian summer monsoon and ENSO interact is that the two phenomena are integral parts of the coupled ocean–land–atmosphere climate system, and it is difficult to consider separately their effects on global climate anomalies. The problem is further complicated by the fact that internal dynamics plays a significant role in Indian summer monsoon variability. Nevertheless, we suggest a mechanism by which Indian summer monsoon variability can affect ENSO variability and provide an explanation for the correlation seen in Fig. 2.

The Indian monsoon is a large sub-tropical heat source which can affect the global circulation. Variability of the monsoon, in turn, is associated with global circulation anomalies. In particular, through shifts in the so-called Walker circulation, it is likely that variability in the Indian summer monsoon leads to anomalies in tropical Pacific wind stress, irrespective of the local SSTA. These anomalies in the tropical Pacific wind stress may force anomalies in the SST, current and thermocline depth. The current and thermocline-depth anomalies result in a temporally and spatially remote response in the SSTA via ocean wave dynamics and coupled air–sea interactions. The question is: are these 'monsoon-forced wind-stress anomalies' robust enough to affect the ENSO variability significantly.

In order to test this hypothesis we start with a simple coupled model confined to the tropical Pacific (Zebiak and Cane 1987) that does not include the effects of a variable monsoon. We then parametrize or prescribe the effects of a variable monsoon in the coupled model. With this parametrization or prescription, the wind-stress anomalies during June to September in the tropical Pacific are due to two processes: (i) coupled air–sea interactions that are restricted to the tropical Pacific, and (ii) large-scale changes in the Walker circulation that are remotely driven by an anomalous Indian summer monsoon. The difference between the coupled-model simulations with and without the effects of the variable monsoon can then be interpreted as the impact of a variable Indian summer monsoon on ENSO.

There are two major difficulties with this approach. First, we need to determine the impact of a variable monsoon on the global circulation and, specifically, the tropical Pacific wind stress that is independent of the internal ENSO dynamics. Second, we need to incorporate this effect into the coupled model. It is not possible to isolate the effects of a variable monsoon that is independent of ENSO from past observations; therefore we use a state-of-the-art atmospheric general-circulation model (AGCM) forced with climatological SST as a lower-boundary condition to infer this relationship. The monsoon also has considerable interannual variability in this simulation. Since the SSTs are climatological in this experiment, the variability of the monsoon is entirely due to internal dynamics, and feedbacks from predicted land surface processes such as soil moisture and snow cover. Using simple statistical techniques we relate the monsoon variability to wind-stress variability over the tropical Pacific. This calculation gives a wind-stress anomaly spatial pattern associated with a variable monsoon. Once the

strength of the monsoon is known, the effects of the monsoon can be incorporated into the coupled model using this wind-stress anomaly pattern.

To incorporate the variable monsoon into the coupled model we apply two different procedures. First, we prescribe or specify the strength of the monsoon. This specification is independent of the evolution of the coupled model. The second procedure is to parametrize the strength of the monsoon in terms of the evolution of the coupled model. To parametrize the strength of the monsoon, we used the contemporaneous correlation seen in Fig. 2. An empirical relationship between contemporaneous east Pacific SSTAs and monsoon-rainfall anomalies is derived. Then, using the coupled model SSTA, a monsoon-rainfall anomaly can be predicted. With either procedure, the spatial pattern of the wind-stress anomalies associated with the variable monsoon is determined *a priori* from the AGCM simulation forced by climatological SST.

Similar to CN, the main focus of this study is on isolating the effects of an anomalous monsoon on the global circulation and incorporating these effects into the Zebiak and Cane (1987) coupled model. In order to do this, CN relied on a rotated principle component analysis of observational data, whereas we used an AGCM forced with climatological SSTs. These differences are discussed in more detail in section 3. Moreover, the focus here is to provide an explanation for the correlation seen in Fig. 2 and to examine how a weak or strong monsoon affects an ongoing warm or cold event.

A series of coupled-model simulations and experiments with and without the effects of a variable monsoon are presented. By prescribing the strength of the monsoon we demonstrate how a weak monsoon can enhance (weaken) an ongoing warm (cold) event. Similarly, a strong monsoon strengthens (weakens) cold (warm) events. It is also shown that, under certain circumstances, a weak monsoon can trigger an El Niño event which otherwise would not have grown into a mature ENSO episode. This does not imply that an El Niño would not occur without the monsoon, but it does suggest that the monsoon fluctuations can trigger an El Niño. In some cases the El Niño occurs a year earlier than if there were no monsoon fluctuations. In multi-decadal simulations with a parametrized monsoon, it is shown that the monsoon enhances the ENSO variability. Moreover, these multi-decadal simulations reproduce the observed lag/lead correlation seen in Fig. 2.

2. The models

Two dynamic models are used in this study. The COLA* AGCM, described below, is used to isolate the effects of a variable monsoon on global circulation anomalies. The AGCM has been extensively used for monsoon studies (e.g. Fennessy *et al.* 1994) and for ENSO studies (Kirtman *et al.* 1997; Kirtman and DeWitt 1997; Kirtman and Zebiak 1997). The Zebiak and Cane (1987) coupled model, also described below, is then used to investigate how the monsoon affects ENSO variability. This simple coupled model has been used for a number of ENSO prediction and predictability studies (e.g. Goswami and Shukla 1991). A version of this model was used by Kirtman (1997) to understand ENSO dynamics, and by Kirtman and Schopf (1998) to study ENSO predictability.

(*a*) *The COLA AGCM*

The atmospheric model used in the experiments described here is the COLA AGCM (more details can be found in Kinter *et al.* (1988), Xue *et al.* (1991) and DeWitt (1996)). The complete model documentation is given by Kinter *et al.* (1997). The model is a global spectral model with triangular truncation at wave number 30. There are

* Center for Ocean–Land–Atmosphere Studies.

18 unevenly spaced σ-coordinate vertical levels. The model includes the simplified biosphere model over land described by Xue *et al.* (1991), the parametrization of the solar radiation is after Lacis and Hansen (1974), and terrestrial radiation follows Harshvardhan *et al.* (1987). The deep convection is an implementation of the relaxed Arakawa–Schubert scheme of Moorthi and Suarez (1992) described by DeWitt (1996). There is a turbulent closure scheme for the subgrid-scale exchange of heat, momentum, and moisture as by Miyakoda and Sirutis (1977) and Mellor and Yamada (1982). A gravity-wave drag parametrization is included in the model, which is described by Kirtman *et al.* (1993).

(*b*) *The coupled model*

The atmospheric dynamics follows Gill (1980), i.e. steady-state, linear shallow-water equations on an equatorial beta plane. Linear dissipation in the form of Rayleigh friction and Newtonian cooling is used. The circulation is forced by a heating anomaly that depends partly on the local SSTA and on low-level moisture convergence. The dynamics of the ocean model is described by linear reduced gravity equations of motion which simulate thermocline-depth anomalies and depth-averaged baroclinic currents. A shallow friction layer of constant depth (50 m) is added to the top of the model to simulate the surface intensification of wind-driven currents. The equation governing the SST includes the effects of horizontal and vertical advection of temperature by both mean and anomalous currents. The annual cycle is included in the model by the prescribed mean current, mean temperature, mean upwelling and mean surface-wind convergence.

There are some well known deficiencies of this coupled model that should be mentioned. First, the amplitudes of cold events tend to be much weaker than in the observational record. Similarly, the model tends to over predict the strength of warm events. The coupled-model simulation is also more regular than the observed time series. Finally, and this is most relevant for this study, the coupled interactions occur too far to the east as compared with observations.

3. The AGCM monsoon without ENSO

As discussed in the introduction, the primary difficulty in understanding how the Indian summer monsoon might affect ENSO is that the two phenomena are coupled, and it is difficult to isolate them. The strategy used here is to force an AGCM with climatological SST, and then, using linear regression, isolate the effect of a variable monsoon on tropical Pacific wind-stress anomalies. The tropical Pacific wind-stress anomaly produced by this calculation is independent of ENSO variability.

Using monthly climatological SST as the lower-boundary condition, the COLA AGCM was integrated for 50 years. Figures 3(a) and (b) show the June–September AGCM climatological mean precipitation over the tropics and its standard deviation, respectively. For comparison, Figs. 4(a) and (b) show the mean and the standard deviation calculated with observed precipitation (Xie and Arkin 1996) from 1979–95. The standard deviation is computed for each month of the year and the values plotted in Figs. 3(b) and 4(b) are the average standard deviations from June to September. It should be also noted that the observations include the effects of interannual variability of SST.

In terms of the large-scale features, the rainfall distribution in the AGCM is realistic. Over the oceans the major inter-tropical convergence zones (ITCZs) are at the correct

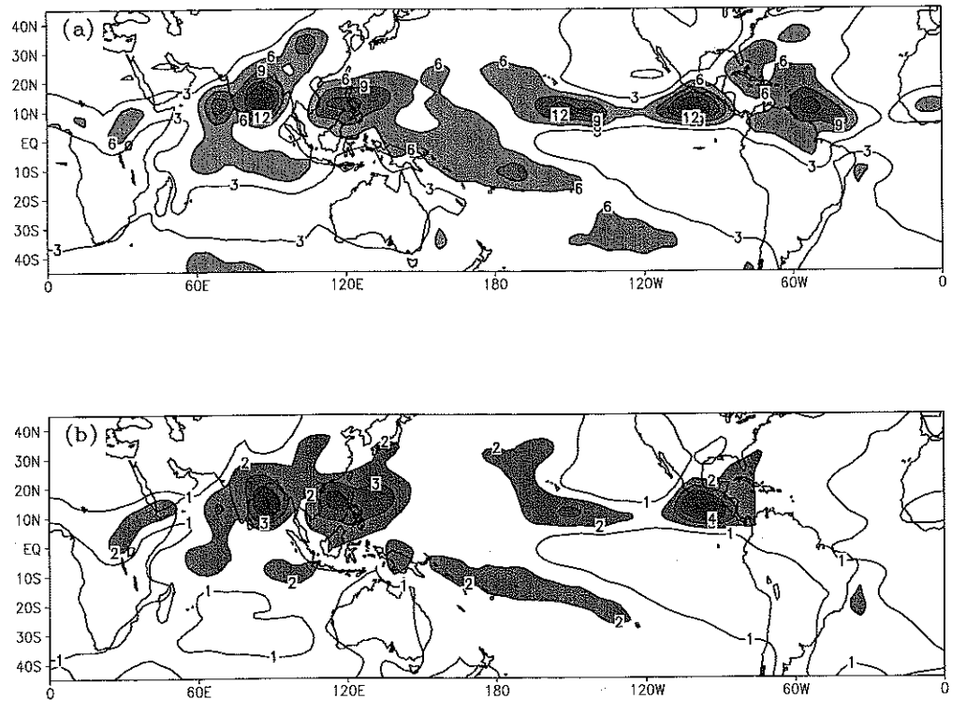

Figure 3. COLA atmospheric general-circulation model June–September precipitation, (a) mean and (b) standard deviation. The contour interval in (a) is 3 mm day^{-1} and in (b) is 1 mm day^{-1}. The standard deviation is computed for each month of the year and the values plotted in (b) are the average standard deviation from June to September. Shading is shown for emphasis.

location and have about the right magnitude. The broad features of the mean Indian–Asian monsoon system are readily apparent, with heavy rainfall over the subtropical east Asian continent and neighbouring oceans. The rainfall associated with the warm pool in the western Pacific is also well simulated.

As is to be expected, some of the smaller-scale features of the monsoon are not as well simulated. The mean Indian monsoon in the AGCM has two strong centres of action over the ocean on either side of the Indian sub-continent. The observations indicate somewhat weaker centres of action, and the rainfall maximum over the Bay of Bengal is further to the north than in the AGCM. Over south-eastern India the observations indicate relatively dry conditions, whereas the AGCM gives a relative maximum. The rainfall maximum along the western Ghats in the observations is more closely aligned with the continental boundary than in the AGCM. The AGCM produces an erroneous rainfall maximum of approximately 6 mm day^{-1} in central western China.

Throughout the tropics the bulk of the interannual variability in precipitation (Figs. 3(b) and 4(b)) is co-located with regions of relatively high mean rainfall in both the observations and in the AGCM. The regions of highest variability are in the Indian–Asian monsoon region and in the oceanic ITCZ. The AGCM overestimates the variability in the ITCZ in the far eastern Pacific, but underestimates the variability in the Atlantic ITCZ. The variability in the warm-pool region of the west Pacific is too low compared with the observations. The AGCM also underestimates the rainfall variability of the Indian Ocean just south of the equator.

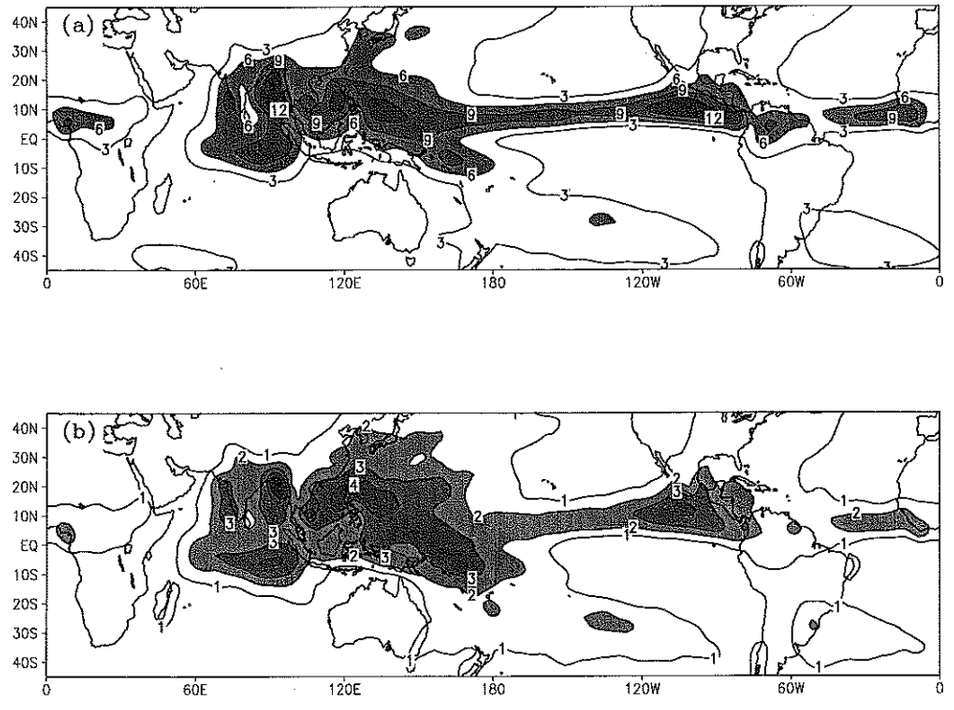

Figure 4. As Fig. 3 but for the Xie–Arkin observed precipitation for June–September 1979–96.

Focusing on the greater Indian monsoon region, the magnitude of the variability is comparable with the observations. This is somewhat surprising, given the fact that the AGCM simulation does not include the interannual variability of the SST. The variability with observed SST has been compared with the simulation with climatological SST, and the two variances are comparable. We do not know whether this is an indication of the model's deficiency in simulating the SST forced monsoon variability, or whether the internal dynamics and feedbacks from land surface processes are sufficient to produce the observed variability. It is well known that this model (and several other models) cannot simulate the observed SST–monsoon rainfall relationship.

Consistent with the observations, the AGCM produces two centres of maximum variability on either side of the Indian sub-continent. As with the mean rainfall, the maximum variability in the Bay of Bengal is displaced too far south compared with the observations. This displacement gives a relative maximum in the land rainfall variability along the south-eastern coast of India where the observations have a minimum. Along the western Ghats the variability in the model is too weak.

Using the AGCM precipitation standard deviation as a guide (Fig. 3(b)), we have defined a monsoon-rainfall anomaly index (MRA) to be the area-averaged rainfall anomaly over 60°E–100°E and 5°N–25°N in mm day^{-1}. Figures 5(a) and (b) show the time series from the 50-year AGCM simulation and the observations from the 16 years available, respectively. The values plotted are for June, July, August and September, all other months are masked out. Again, we see that the AGCM variability is comparable with the observed variability. In both the observations and the model it is possible to have monthly anomalies of both signs in any given year. It is also possible that several

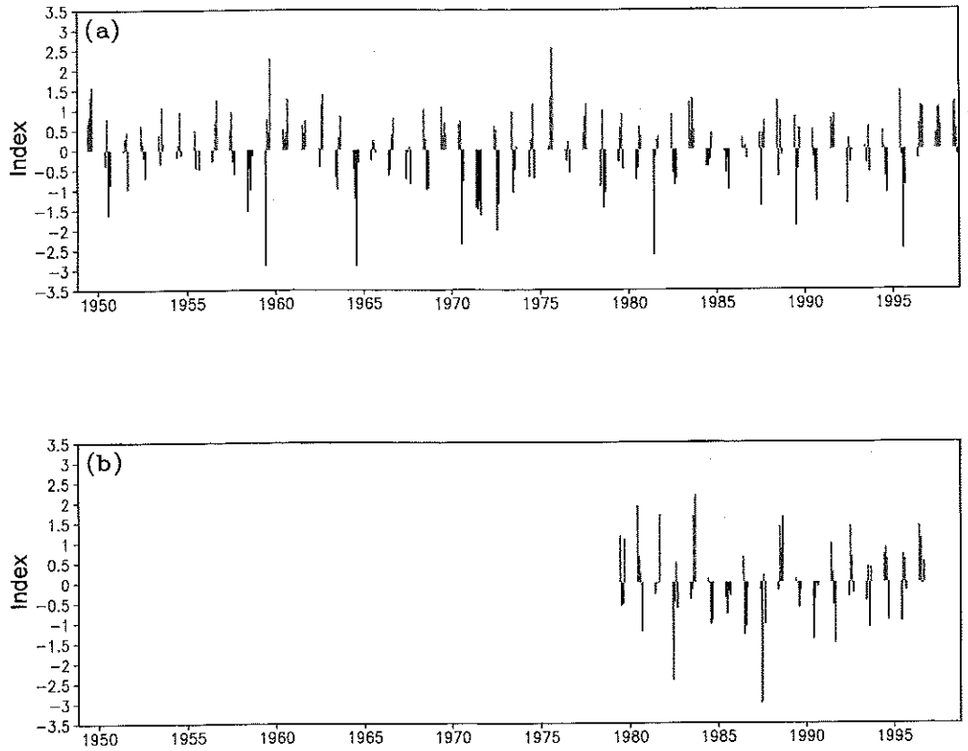

Figure 5. Time series of area averaged (60°E–100°E, 5°N–25°N) monsoon-rainfall anomaly index for (a) 50 years of atmospheric general-circulation model simulation with climatological sea surface temperature and (b) Xie–Arkin observed precipitation.

consecutive years are either anomalously weak or strong. For example, in the AGCM simulation, years 1960–63 have positive anomalies and in the observations 1995–97 have positive anomalies.

In order to calculate the global AGCM circulation anomalies associated with the monsoon-rainfall anomalies, we applied simple linear regression. The 50-year MRA time series (Fig. 5(a)) is regressed onto the zonal wind and zonal wind-stress anomalies in Figs. 6(a) and (b), respectively. The contours show the results of the regression, and the shaded regions indicate areas where the regression coefficients are significant at the 95% confidence level using a Student's t-test (Devore 1982). For comparison, Figs. 7(a) and (b) show the corresponding climatological fields simulated by the AGCM. Figure 6(a) shows the vertical structure of the zonal wind anomaly along the equator that corresponds to an MRA value of 2 mm day^{-1}. Along the equator the response is largest over the Indian Ocean and in the central and eastern Pacific. Over the Indian Ocean at the surface there are enhanced easterlies. These enhanced easterlies at the equator correspond to a strengthening of the low-level cross-equatorial circulation that is typical of a relatively strong Indian summer monsoon. In the upper troposphere the easterlies along the equator are enhanced by about 15%, which is also typical of an enhanced Indian summer monsoon.

Over the central and eastern Pacific Ocean the climatological flow is easterly in the lower troposphere, which weakens with increasing height and becomes westerly

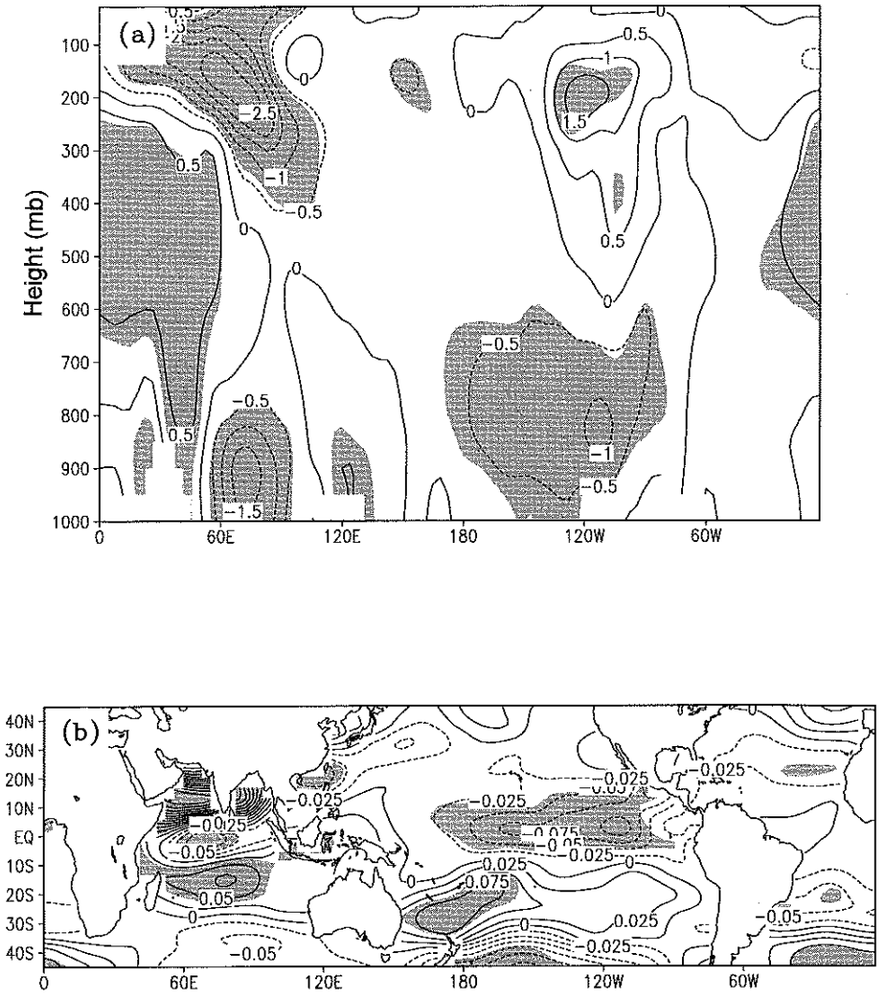

Figure 6. Linear regression of the monsoon-rainfall anomaly index on the (a) atmospheric general-circulation model zonal wind anomaly along the equator and (b) zonal wind-stress anomaly. The amplitude of the patterns corresponds to a rainfall anomaly of 2 mm day^{-1}. The contour interval in (a) is 0.5 m s^{-1} and in (b) is 0.025 dynes cm^{-2}. See text for explanation of the shaded regions.

near the tropopause (Fig. 7(a)). With a strong monsoon the strength of the low-level easterlies and the upper-level westerlies is enhanced. The net effect is that during a strong Indian summer monsoon the Walker circulation over the tropical Pacific is enhanced, and during a weak monsoon the strength of the Walker circulation is reduced. This relationship is independent of any local SST variability in the tropical Pacific.

The climatological and the anomalous zonal wind stresses are shown in Figs. 7(b) and 6(b), respectively. As expected, with an enhanced summer monsoon the westerly flow across the Indian sub-continent is stronger than normal. Along the equator in the Indian Ocean there are easterly anomalies, and south of the equator the climatological easterly flow is reduced by as much as 10%. Similar to the Indian Ocean, the easterly flow south of the equator in the Pacific is reduced with a stronger than normal monsoon.

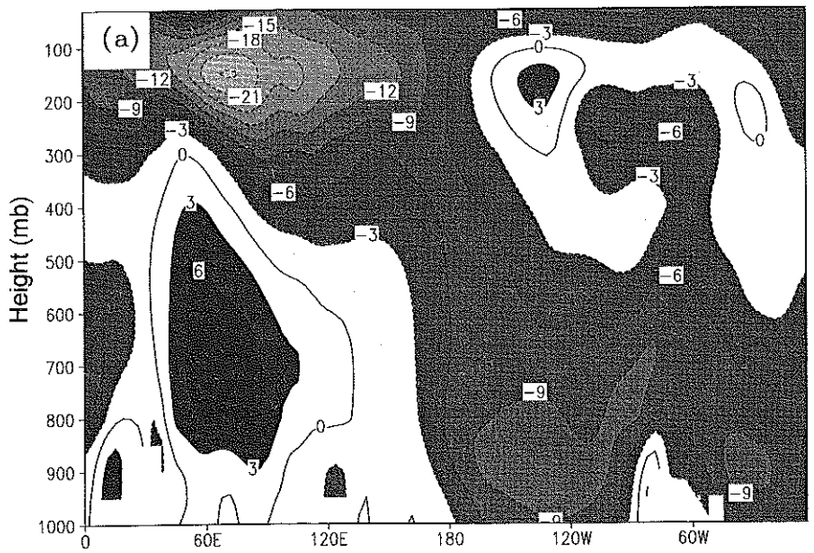

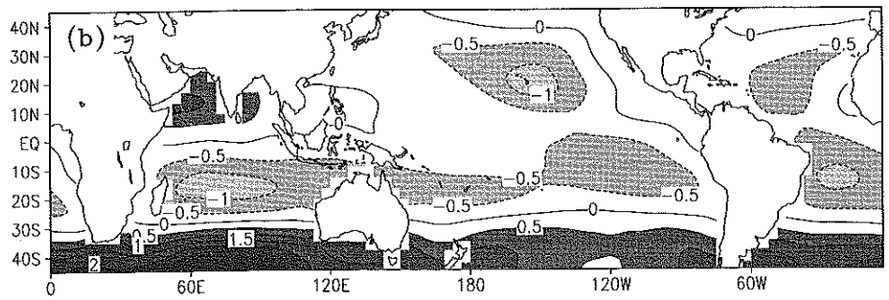

Figure 7. Atmospheric general-circulation model (a) zonal wind climatology along the equator and (b) zonal wind-stress climatology. The contour interval in (a) is 3 m s^{-1} and in (b) is 0.5 dynes cm^{-2}. Shading is shown for emphasis.

In the equatorial zone throughout most of the central and eastern Pacific there are easterly wind-stress anomalies. Even though there are no SSTAs in this AGCM simulation, the zonal wind-stress anomalies in the tropical Pacific associated with either a stronger or weaker-than-normal monsoon are consistent with the usual contemporaneous ENSO–monsoon relationship discussed in the introduction. In other words, during an anomalously strong monsoon the simultaneous easterly wind-stress is stronger than normal and the SSTA is below normal in the eastern Pacific. Based on these AGCM results alone, it is reasonable to speculate that a variable monsoon should have a positive feedback to ENSO variability.

In addition to the results of the *t*-test, the significance of the anomalies shown in Figs. 6(a) and (b) can be assessed by comparing the anomalies with the standard deviation. The standard deviation, in the same format as Figs. 6(a) and (b), is plotted

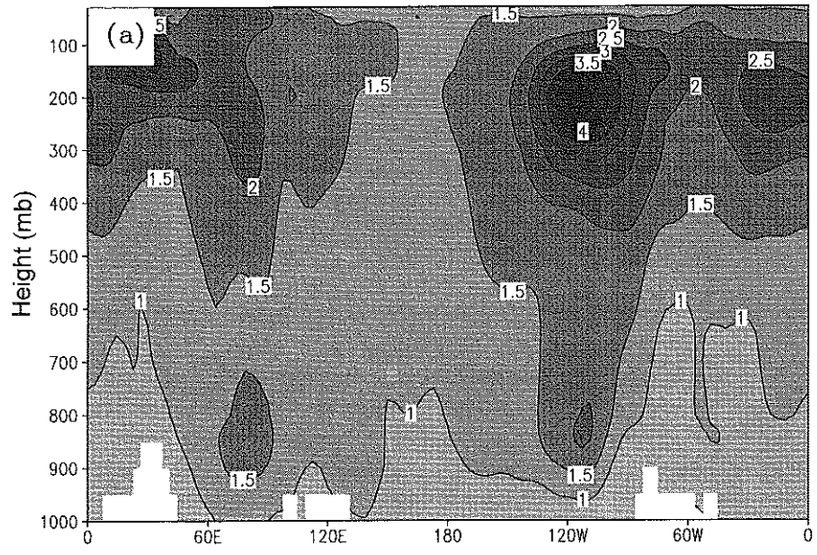

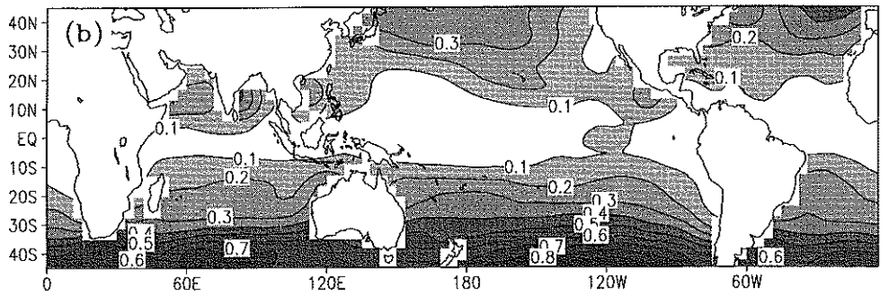

Figure 8. Atmospheric general-circulation model standard deviation for (a) zonal wind anomalies along the equator and (b) the zonal wind-stress anomalies. The contour interval in (a) is 0.5 m s^{-1} and in (b) is 0.1 dynes cm^{-2}. Shading is shown for emphasis.

in Figs. 8(a) and (b). Within the monsoon region, both at the surface and throughout the troposphere, the variability associated with the monsoon (Figs. 6(a) and (b)) is comparable with the total variability. In the tropical Pacific the variability of the Walker circulation associated with the monsoon is about half of the total variability. At the surface, near the equator, the total variability is generally less than 0.1 dyne cm^{-2}, whereas the variability due to the monsoon is between 0.05 and 0.1 dyne cm^{-2} for most of the central and eastern tropical Pacific. We also recomputed the linear regression with a number of 20-year sub-samples of the 50-year record. The anomalies calculated with these 20-year sub-samples were quantitatively similar to the anomalies shown in Figs. 6(a) and (b). Based on the *t*-test and comparisons with the standard deviation, we conclude that the wind-stress anomalies in the central and eastern Pacific forced by the monsoon variability are significant.

At this stage it is worth noting some differences in how we have isolated the impact of a variable monsoon in comparison with CN. In our calculation the circulation anomalies associated with the variable monsoon are determined from an AGCM simulation and are necessarily independent of any SSTA. CN, on the other hand, used observational data to derive monsoon-heating anomalies that are necessarily related to tropical Pacific SSTAs. These monsoon-heating anomalies were then used to force a Gill (1980) type atmosphere model. The major difference in the result is that our 'monsoon wind-stress anomalies' are largest in the eastern and central tropical Pacific, whereas the monsoon wind-stress anomalies in CN are confined to the far western Pacific. In fact the CN monsoon wind-stress anomalies are negligible in the central and eastern Pacific. These structural differences may affect how the coupled model responds to the monsoon wind-stress anomalies. For example, Xue *et al.* (1997) and Chen *et al.* (1997), using a singular vector decomposition analysis, find that wind perturbations in the central and eastern Pacific give the 'fastest' divergence of solutions (or error growth). Conversely, Moore and Kleeman (1997) find that perturbations in the western Pacific are most efficient in perturbing the coupled system. Given that the model used here is the same as Xue *et al.* (1997), it is expected that perturbations in the central and eastern Pacific will be most effective in perturbing the coupled model, but this is a model-dependent result.

4. Incorporating a variable monsoon in the coupled model

The purpose of the analysis of the previous section was to isolate the wind-stress anomalies in the tropical Pacific that are associated with a variable monsoon, but that are also independent of local SSTA forcing. In this section we describe how these wind-stress anomalies were incorporated into the coupled model. The intent is to compare two coupled-model simulations where the difference between these two simulations is isolated to the impact of the variable monsoon. Two separate procedures were used to incorporate the monsoon into the coupled model. The first was to prescribe the strength of the monsoon and the second was to parametrize the strength of the monsoon using the simulated SSTA in the eastern Pacific. Results for the prescribed monsoon are presented in section 5, and for the parametrized monsoon in section 6. With either the prescription or the parametrization, the wind-stress anomalies during June to September in the tropical Pacific are due to two processes: (i) coupled air–sea interactions that are restricted to the tropical Pacific, and (ii) large-scale changes in the Walker circulation that are remotely driven by an anomalous Indian summer monsoon.

Without any modifications, the coupled model used here is restricted to the tropical Pacific, and the atmospheric component is a steady-state model; therefore, the wind-stress anomalies are due to local-heating anomalies and SSTAs. We refer to these wind-stress anomalies, which are independent of the monsoon, as $\boldsymbol{\tau}_{\text{pac}}$. The wind-stress anomalies in the tropical Pacific that are due to the prescribed or parametrized monsoon, but are also independent of local-heating anomalies and SSTAs are referred to as $\boldsymbol{\tau}_{\text{mon}}$. In the simulations described here the total wind stress is given by

$$\boldsymbol{\tau}_{\text{total}} = \boldsymbol{\tau}_{\text{pac}} + \boldsymbol{\tau}_{\text{mon}}. \tag{1}$$

In the control simulations $\boldsymbol{\tau}_{\text{mon}}$ is identically zero for all months, and in the simulations that include the monsoon $\boldsymbol{\tau}_{\text{mon}}$ is non-zero only during June through to September. The spatial pattern of $\boldsymbol{\tau}_{\text{mon}}$ is the same in all the experiments and is given by the linear regression discussed in section 3. Figure 6(b), for example, shows the spatial structure of the zonal component of $\boldsymbol{\tau}_{\text{mon}}$ given a monsoon rainfall anomaly of 2 mm day^{-1}. In the coupled-model experiments, the amplitude of $\boldsymbol{\tau}_{\text{mon}}$ is either specified or parametrized using the coupled-model SSTA in the eastern Pacific.

With this formulation, prescribing or parametrizing the effects of the monsoon is reduced to prescribing or parametrizing the contemporaneous MRAs. In order to parametrize the MRA, we use the fact that, in the observational record, NINO3 SSTAs during June–September are well correlated (−0.6) with all-India rainfall anomalies (see Fig. 2). Regressing the all-India rainfall data from 1871 to the present onto the observed NINO3 SSTA from GISST2.3a indicates that for a 1.0 degC NINO3 anomaly the all-Indian rainfall anomaly is −0.7 mm day^{-1}. Using this relationship,

$$\boldsymbol{\tau}_{\text{mon}} = \text{MRA}\mathbf{f}(x, y) \tag{2}$$

$$\text{MRA} = \alpha\text{NINO3} \tag{3}$$

where $\mathbf{f}(x, y)$ is the spatial pattern of the wind-stress anomalies in dynes cm^{-2} (mm day^{-1})$^{-1}$ and $\alpha = -0.7$ mm day^{-1}K^{-1}. The parametrization given by (2) and (3) overemphasizes the influence of ENSO on the monsoon because we have assumed a perfect correlation. This issue is explored in some detail in section 6. To specify $\boldsymbol{\tau}_{\text{mon}}$, (3) is bypassed and the MRAs are prescribed during the summer monsoon season. We use an MRA value of ±2 mm day^{-1} in all the prescribed monsoon simulations described in the next section.

The relationship between NINO3 SSTA and all-India rainfall anomalies is not perfect (Fig. 2), and there are El Niño years in which the monsoon-rainfall anomalies are above normal (Fig. 1(b)). There are also years in which the monsoon-rainfall anomalies are large, but there are no significant SSTAs in the tropical Pacific. These possibilities will be explored in the case-studies described in the next section by specifying the MRA. We also address the question of whether the monsoon can trigger El Niño events.

5. Prescribed monsoon

We first ran the coupled model without the effects of the monsoon for 200 years. In order to sample various phases of the ENSO cycle, we selected several different January initial conditions from this control simulation and integrated the coupled-model for shorter periods with a specified value of the MRA included that was independent of the evolution of the coupled-model SSTA. The five examples shown below are indicative of a much larger sample of experiments. First, we choose a warm ENSO event in the control integration and show how a prescribed weak monsoon (MRA = −2 mm day^{-1}) and a prescribed strong monsoon (MRA = 2 mm day^{-1}) affect the evolution of that warm ENSO event. Second, we apply the same approach to a cold event in the control integration. Finally, we show an example of how a weak monsoon can trigger an El Niño to occur one year earlier than without the effects of the monsoon.

(*a*) *A prescribed monsoon and warm ENSO*

Figures 9(a) to (d) show the time evolution along the equator of a warm ENSO event with and without the effects of the specified weak monsoon. In this case, in (2) we have specified a weak monsoon (MRA = −2.0 mm day^{-1}) for the entire monsoon season from June to September. Initially, the SSTA in the eastern Pacific is near normal, and during the monsoon season (months 6–9) the SSTA is greater than 1.0 degC over most of the eastern and central equatorial Pacific. The warm event peaks during months 10–12, but remains relatively warm through to month 18. Figure 9(a) shows the evolution of the

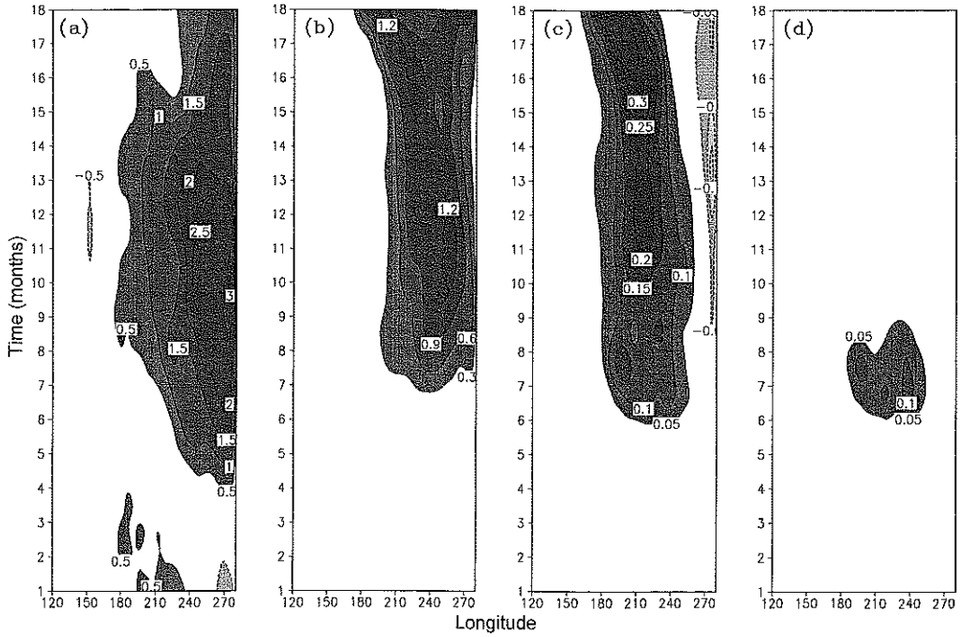

Figure 9. Time–longitude cross-section for months 1–18 along the equator for a warm ENSO event of (a) sea surface temperature anomaly (SSTA) without the monsoon, (b) SSTA difference for the simulation with a weak monsoon minus the simulation without the monsoon, (c) zonal wind-stress anomaly difference for the simulation with a weak monsoon minus the simulation without the monsoon and (d) the zonal wind-stress forcing due to the weak monsoon only. The contour intervals are (a) 0.5 degC, (b) 0.3 degC, and (c) and (d) 0.05 dynes cm^{-2}, respectively. Shading is shown for emphasis.

SSTA in the control coupled integration without the effects of the monsoon. Figures 9(b) and (c) show the SSTA and zonal wind-stress difference between the simulation with and without the prescribed monsoon. Figure 9(d) shows the zonal wind-stress due to the monsoon only, τ_{mon}. Both simulations start in January with identical initial conditions.

The zonal component of τ_{mon} along the equator during the monsoon season is westerly (Fig. 9(d)). The zonal component of τ_{pac} is also westerly so that the anomalous monsoon increases the zonal component of τ_{total} felt by the ocean model. This monsoon wind-stress forcing leads to an overall enhancement of the warm event (Fig. 9(b)). SSTA differences first become apparent during the middle of the monsoon season (months 7–8); however, the largest differences are well after the monsoon. From the SSTA differences it can also be seen that the duration of the warm event is lengthened. During the peak phase of the warm event (months 10–12), the SSTAs are increased by as much as 33%. There is a localized eastern Pacific maximum of approximately 1.0 degC in the SSTA difference during months 10–12. This localized maximum difference in the SSTA following an anomalously weak monsoon is consistent with the correlation seen in Fig. 2 where the monsoon leads the SSTA in the east Pacific.

The zonal wind-stress anomalies associated with this specified monsoon (Fig. 9(d)) are relatively small in comparison with the total zonal wind-stress anomalies. The direct effect of the zonal component of τ_{mon} is to deepen the thermocline in the eastern Pacific. This thermocline perturbation is relatively small, and in uncoupled simulations leads to small SSTA differences (less than 0.3 degC). However, in the coupled model, small

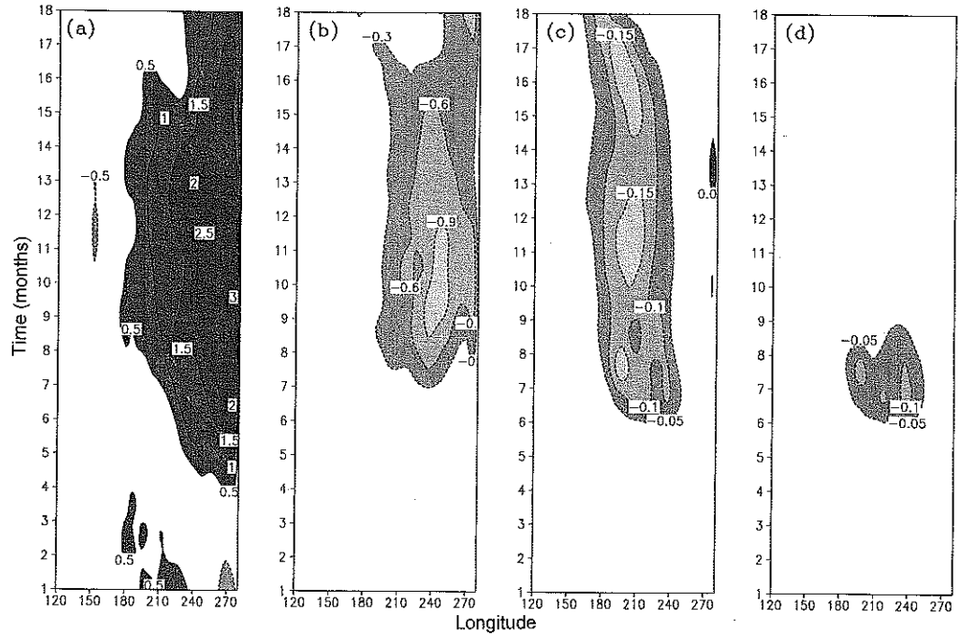

Figure 10. As Fig. 9 but for the strong monsoon.

changes in the SSTA are amplified so that two to four months after the monsoon there are relatively large differences in the SSTA. The monsoon forcing, τ_{mon}, introduces a small perturbation into the coupled tropical Pacific ENSO system. Because this coupled system is unstable, this perturbation leads to a relatively large response later in the simulation.

In the same format as Figs. 9(a)–(d), Figs. 10(a)–(d) show the evolution of the same warm event (Figs. 9(a) and 10(a) are therefore identical) except, in this case, a relatively strong monsoon is prescribed (MRA = 2.0 mm day^{-1}). In this case the zonal component of τ_{mon} along the equator is easterly (Fig. 10(d)) which will weaken the zonal component of τ_{total} felt by the ocean model. As expected, a strong monsoon decreases the warm SSTA in the eastern Pacific. Again, the importance of the coupling between the ocean and atmosphere can be seen as the maximum response is to two to four months after the monsoon. Comparison of Figs. 9(b)–(d) and 10(b)–(d) indicates that there is some symmetry between the response with a strong and weak monsoon. For example, the largest response is temporally remote from the monsoon forcing and confined to the eastern Pacific. However, the magnitude of the response is stronger in the case of a weak monsoon.

(*b*) *A prescribed monsoon and cold ENSO*

In the coupled model, the evolution of the simulated warm and cold ENSO events is asymmetric. This asymmetry can best be seen in the magnitude and duration of the ENSO events. The warm events, for example, consistently have larger magnitude and last several months longer. The phase locking of cold events with the annual cycle is also different than with warm events. The observational record shows similar asymmetries. Given this asymmetry in the model, we expect the impact of the specified monsoon

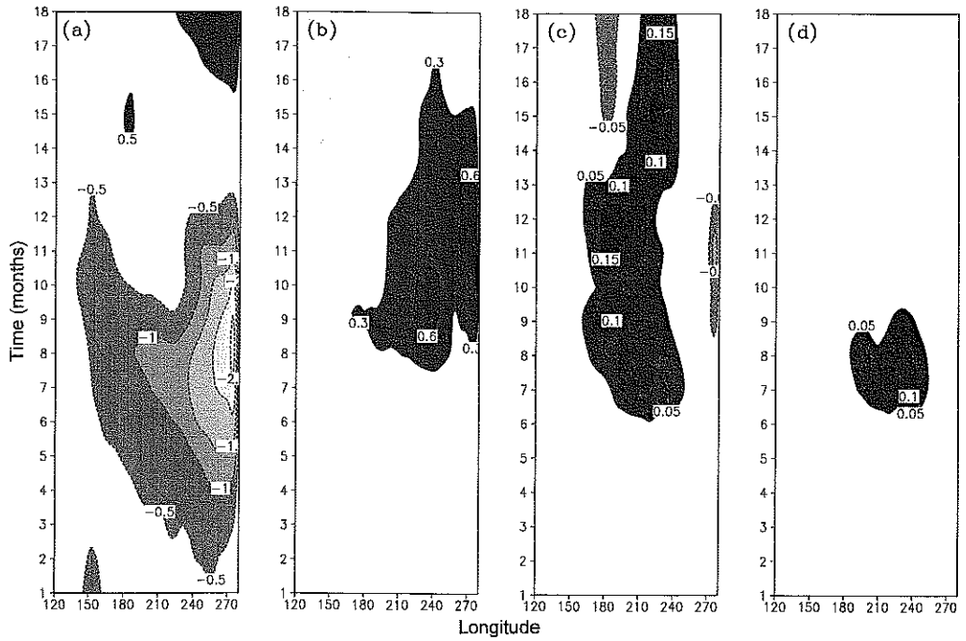

Figure 11. Same as Fig. 9 except for a cold ENSO event.

during a cold event to be different than during a warm event. Using the same procedure as above, we have specified either a weak or strong monsoon during a cold event in the control integration.

Figures 11(a)–(d) show the time evolution of a cold event with and without a prescribed weak monsoon. As with the warm event, initially the SSTA in both simulations is near normal. Cold anomalies, however, develop and peak about two months earlier than with the warm event. The SSTAs are also more tightly confined to the eastern Pacific. In this case, the timing of the monsoon forcing is largely in phase with the coldest SSTA (see Figs. 11(a) and 11(d)). Prescribing a weak monsoon tends to weaken the cold event although the impact is not as large as in the case of a warm event. As with the warm event, the maximum response is two to four months after the monsoon season.

Figures 12(a)–(d) show the impact of a strong monsoon on the evolution of this cold event. Although the response is of the opposite sign, the SSTA differences during months 8–11 are similar in structure and evolution to the case with a weak monsoon. A strong monsoon tends to strengthen the cold event further. Compared with the warm-event cases, the impact of the monsoon on the cold event is relatively small. We have repeated these experiments for a number of different cases and found that the effect of the monsoon is systematically weaker during cold events. There is some suggestion that the magnitude of cold events in this coupled model is underpredicted (Kirtman and Zebiak 1997), and it remains to be determined if this asymmetry in the response to the monsoon is a systematic problem with the model or due to some inherent difference between warm and cold events.

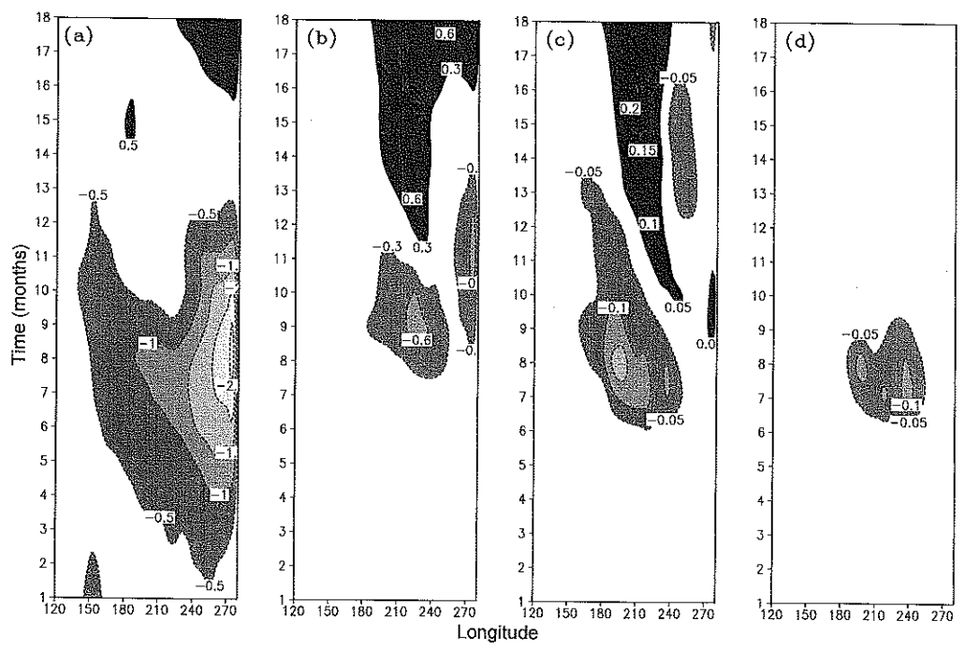

Figure 12. Same as Fig. 10 except for a cold ENSO event.

(c) *The monsoon as an El Niño trigger*

One interesting aspect of Figs. 12(a)–(d) is that there is some indication that the forcing due to the strong monsoon during the cold event leads to earlier development of the following warm event. This can be seen during months 12–18 where the SSTA difference (Fig. 12(b)) and the zonal wind-stress anomaly difference (Fig. 12(c)) are both positive. This leads to the question of whether an anomalous monsoon can trigger the development of an ENSO event. We address this question in the example shown below. In selecting this particular example, we have chosen an initial state from the control run that was, in some sense, preconditioned to transition into an El Niño, yet for some reason the warm event was delayed by 12 months. By introducing the anomalous monsoon forcing, the warm event occurs 12 months earlier and is considerably stronger.

Figures 13(a) and (b) show the 36-month evolution along the equator of the SSTAs and thermocline anomalies for the control simulation, respectively. During the first 12 months of this simulation there are modest cold SSTAs in the eastern Pacific. During months 12–16 the eastern Pacific returns to near-normal temperatures, and a weak positive SSTA develops in the central Pacific. As the cold SSTAs in the eastern Pacific reach their peak (months 6–10), a thermocline depression in the western Pacific develops. Beginning in about month 10, this western Pacific thermocline depression appears to migrate eastward into the central Pacific where weak positive SSTAs develop. However, large-scale eastern Pacific warming does not begin until several months later, and mature El Niño conditions do not occur until months 30–36. The precise reason why the warm event was delayed by 12 months is not known, but, as shown here, a weak monsoon can act as a trigger leading to the earlier development of the warm event.

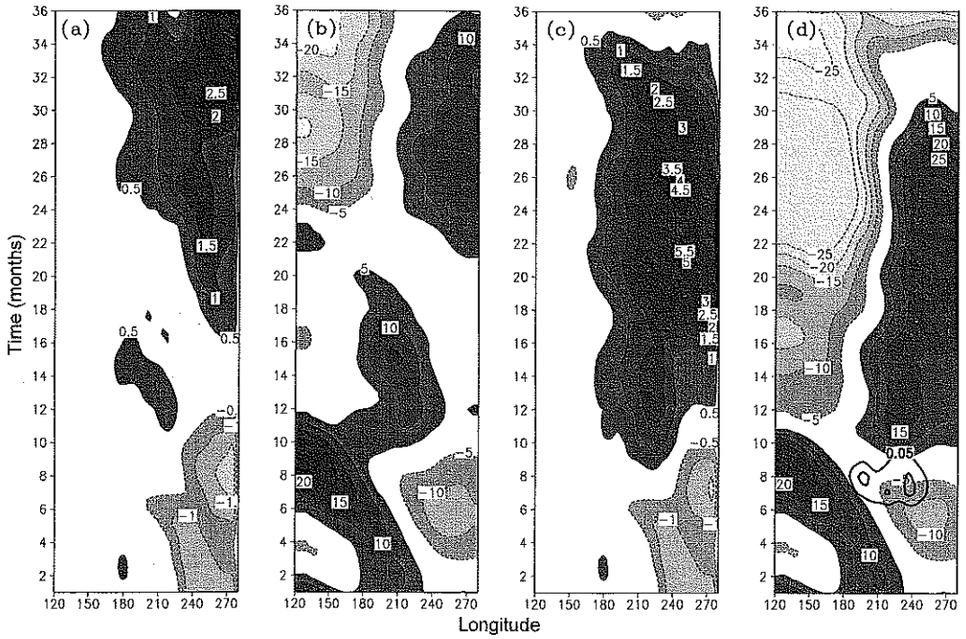

Figure 13. Time–longitude cross-section for months 1–36 along the equator of (a) sea surface temperature anomaly (SSTA) without the monsoon, (b) thermocline anomaly without the monsoon, (c) SST with a weak monsoon, and (d) thermocline anomaly with a weak monsoon. In (d) the monsoon forcing is shown in bold contours during months 6–9. The SSTA contour interval is 0.5 degC and the thermocline anomaly contour interval is 5 m. Shading is shown for emphasis.

Figures 13(c) and (d) show the SSTAs and thermocline anomalies for the simulation with a weak monsoon. The wind-stress forcing associated with a weak monsoon (MRA $= -2$ mm day^{-1}) is included only during months 6–9 and can be seen as the bold contours on Fig. 13(d). The initial evolution of the SSTAs and thermocline anomalies (months 1–5) is identical to the control run. During the monsoon season there is a weakening (approximately 0.3 to 0.6 degC) of the cold SSTA in the eastern Pacific. Consistent with these SSTA differences in the eastern Pacific, the thermocline anomaly in the east is also weaker. Subtle changes in the thermocline anomaly in the west can also be detected.

The most dramatic differences begin after month 10. In the simulation with the monsoon forcing, strong positive central and eastern Pacific SSTAs begin to develop in month 10. At the same time, the thermocline in the east (west) deepens (rises). By months 18–26 a strong El Niño has developed, and by month 34 the eastern Pacific has returned to near-normal conditions. In contrast, the control simulation is in a mature El Niño state during month 34.

6. Parametrized monsoon

The specified monsoon experiments of the previous section indicate how a prescribed variable monsoon affects the evolution of a particular warm and cold event. However, there is considerable observational and modelling evidence that the strength of the monsoon is also affected by the SSTA. In other words, if an anomalous monsoon

modifies the ENSO cycle, the modified ENSO cycle in turn can affect the contemporaneous and subsequent monsoon. However, we have not addressed this question because we have not used a truly coupled ocean–land–atmosphere model. Therefore, to address the coupled ENSO–monsoon feedback and the overall variability of the coupled system we use the parametrization given by (2) and (3) in section 4. First, the case where the amplitude of the monsoon is perfectly predicted is presented. Then we examine how a random component in the MRA affects the coupled system.

A multi-decadal simulation incorporating the parametrized monsoon given by (2) and (3) is compared with a control simulation without the monsoon. With this parametrization we are assuming that the monsoon can be consistently predicted in terms of the contemporaneous SSTA in the eastern Pacific. This is clearly not the case with the real climate system; nevertheless, this parametrized monsoon does isolate the component of the monsoon that is related to the SSTA in the east Pacific, and how this component ultimately affects the variability of the coupled system.

The coupled model both with and without the empirical monsoon was integrated for 300 years. The first 100 years of the simulation is neglected in all the results presented here. Figure 14(a) shows a time–longitude cross-section along the equator of the difference in the SSTA variance between the control simulation (without the monsoon) and the simulation with the parametrized monsoon. Including this parametrized monsoon increases the SSTA variance during the boreal autumn and winter and, surprisingly, decreases the variance during the boreal spring and summer. The largest change is the enhanced SSTA variability during late autumn and early winter, approximately two to four months after the monsoon. At the eastern boundary the SSTA variability is reduced throughout the annual cycle. In a format similar to that of Fig. 14(a), Fig. 14(b) shows the variance in the zonal component of τ_{mon}. The phase lag between the monsoon wind-stress forcing in the central Pacific and the SSTA in the eastern Pacific is readily apparent.

While Fig. 14(a) shows how the parametrized monsoon affects the amplitude of the SSTA variability, Fig. 15 indicates how the parametrized monsoon affects the spectral characteristics of the variability. The NINO3 SSTA spectral density for the control simulation without the monsoon, with the monsoon, and for the GISST2.3a observations are shown in Fig. 15. The spectral density calculation is based on the Fourier method. For additional details the reader is referred to Jenkins and Watts (1968). The observed spectral density has a relatively broad red spectrum with dominant periods between three and five years. In the control simulation without the parametrized monsoon there is a comparatively strong spectral peak at a period of 48 months. The incorporation of the parametrized monsoon broadens the spectrum, particularly towards higher frequencies. Although there is more power at lower frequencies in the simulations with the monsoon, both model simulations underestimate the amplitude at very low frequencies.

Finally, we return to the correlation shown in Fig. 2. To calculate the correlation we define a monsoon wind-stress index to be the area average (160°W–110°W, 5°S–5°N) of the zonal component of τ_{mon}. Figure 16 shows the correlation between this wind-stress index and NINO3 SSTA for the coupled-model simulation with the parametrized monsoon. Overall, the magnitude of the correlation is larger than with the observations, but the basic structure is similar. The larger correlation occurs because the parametrized monsoon is perfectly predictable and is not inherently chaotic. Unlike the observations, the correlation is negative for all lags and leads but, like the observations, approaches zero for large lags and leads. In the simulation, the correlation rapidly becomes negative with the SSTA leading the monsoon by about nine months. The negative turn occurs at about six months in the observations. As expected, the contemporaneous correlation is

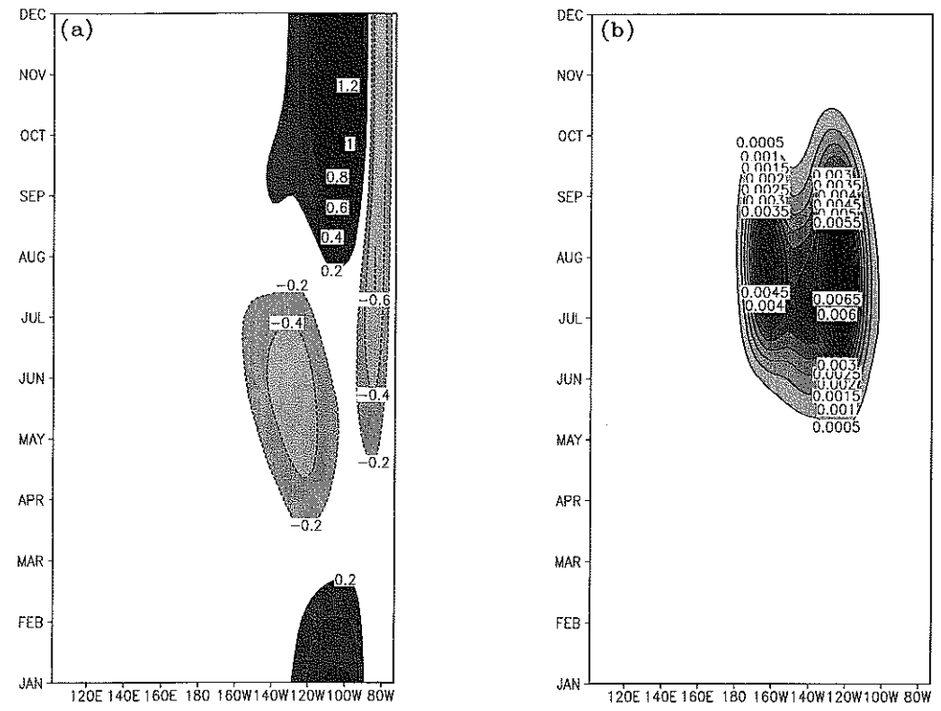

Figure 14. (a) Time–longitude cross-section of sea surface temperature anomaly variance difference between the simulation with the parametrized monsoon and the simulation without the monsoon. The variance is calculated as a function of the annual cycle and the contour interval is 0.2 $degC^2$. (b) Time–longitude cross-section of the variance of the monsoon wind-stress forcing in the parametrized monsoon simulation. The contour interval is 5×10^{-4} (dynes $cm^{-2})^2$. Shading is shown for emphasis.

stronger than in the observations. The most interesting aspect of Fig. 16 is that, similar to the observations, the maximum negative correlation occurs with the monsoon leading the SSTA in the east Pacific by two to four months.

There are two additional curves on Fig. 16. One curve shows the correlation for the case in which the monsoon (or MRA) is completely random and independent of NINO3 SSTA. The standard deviation of the random MRA is chosen to be the same as in the case where the MRA is determined from the NINO3 SSTA. As expected, in the case of a random monsoon the correlation is negligible; however, there is weak negative correlation (−0.18) for NINO3 SSTAs occurring about 3 months after the monsoon season that passes a statistical significance test at the 95% level. The third curve in Fig. 16, which most resembles the observed curve in Fig. 2, is calculated from a simulation where 35% of the amplitude of the MRA is determined from NINO3 SSTA (via Eqs. (2) and (3)) and 65% is random (i.e. independent of NINO3 SSTA). The choice of 35% was based on the well known fact from observations that the correlation between NINO3 SSTA and MRA is about 0.5–0.6. The implication is that even when the relationship between parametrized monsoon and the NINO3 SSTA is significantly degraded (i.e. 65% noise), the observed preference for maximum correlation to occur three to four months after the monsoon is reproduced in the model.

The ENSO, in both observations and in the model, is phase locked to the annual cycle and has its peak amplitude during the boreal winter season. With respect to Fig. 2

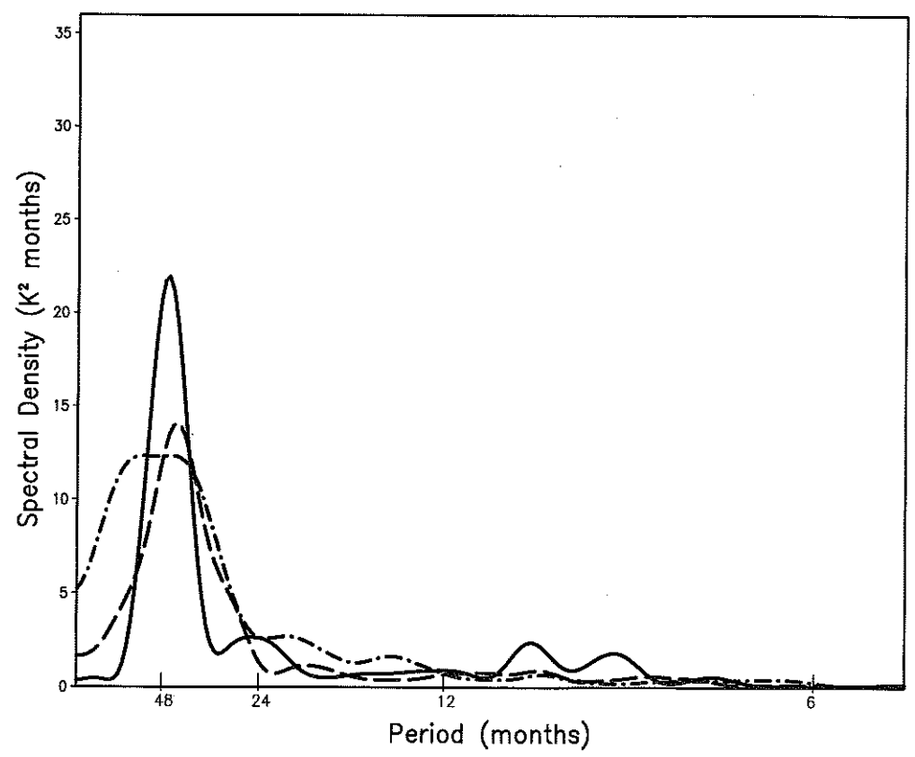

Figure 15. NINO3 sea surface temperature anomaly power spectra of the coupled-model simulation without the monsoon (solid curve), coupled-model simulation with the parametrized monsoon (dashed curve), and the observations (dot-dashed curve).

and Fig. 16, this raises the question of whether the correlation is maximum after the monsoon because this is the time period when the ENSO signal-to-noise ratio is largest. This should not be the case because the correlation by definition is normalized by the square root of the variance of NINO3 SSTA and the monsoon. Nevertheless, in order to test this possibility in the model, we have repeated the parametrized monsoon experiment, except in this case we have shifted the monsoon to be centred during the December–March season as opposed to the June–September season. The correlation was then calculated (not shown) and was found to be very similar to the solid curve in Fig. 16. This suggests that the asymmetry in the correlation is not due to the phase locking with the annual cycle, but is determined by how long it takes for the coupled system to respond to the 'monsoon wind-stress anomalies'.

7. Concluding Remarks

The motivation for the research presented here was to investigate how Indian summer monsoon variability affects ENSO. Specifically, we put forth the hypothesis that Indian monsoon variability forces tropical Pacific wind-stress variability, irrespective of any SSTA in the tropical Pacific. In the coupled ocean–atmosphere climate system these 'monsoon wind-stress anomalies' lead to a temporally and spatially remote response in the SSTA via ocean wave dynamics and coupled air–sea interactions. In order to

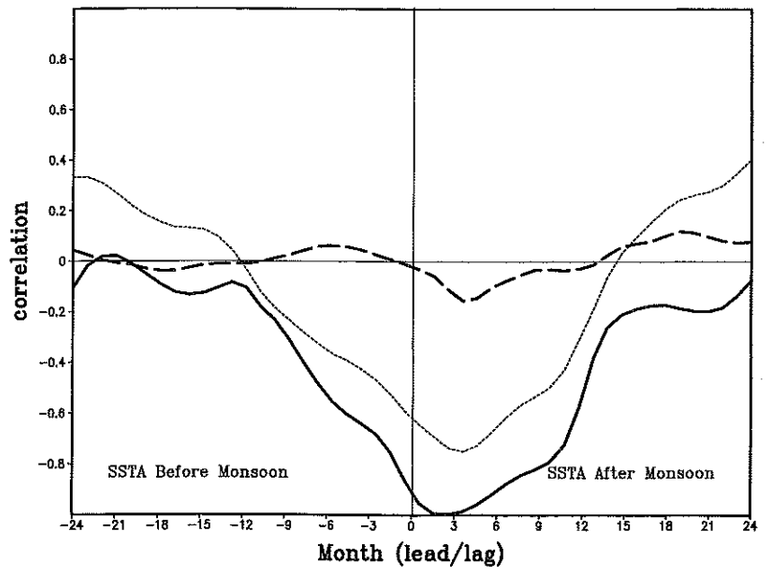

Figure 16. Lag/lead correlation between area-averaged monsoon wind-stress forcing anomalies (160°W–110°W, 5°S–5°N) and NINO3 sea surface temperature anomaly (SSTA) in the coupled-model simulation with the parametrized monsoon (solid curve), a random monsoon (long-dashed curve) and a degraded (see text) parametrized monsoon (short-dashed curve).

test this hypothesis we used an AGCM forced with climatological SST to determine the monsoon wind-stress anomalies, and then incorporated these wind-stress anomalies into the Zebiak and Cane (1987) coupled model.

The results presented here indicate that monsoon variability has a profound effect on ENSO, particularly three to six months after the monsoon season ends. We found that a weak (strong) monsoon enhances (reduces) the magnitude of an ongoing warm ENSO event three to six months after the monsoon ends. Similarly, a strong (weak) monsoon enhances (reduces) the magnitude of an ongoing cold ENSO event. Coupled air–sea interactions in the tropical Pacific are a critical component in amplifying the effect of the monsoon. The contemporaneous and direct (uncoupled) effect of the monsoon forcing is relatively small; however, the temporally remote response is relatively large due to coupled air–sea interactions.

We also showed, given the appropriate initial state, how the monsoon can trigger an El Niño to occur one year earlier than without the effects of the monsoon. This does not imply that the monsoon forces the ENSO; the coupled model has ENSO events even without the monsoon. However, these results do indicate that the monsoon can both enhance ENSO variability and trigger ENSO events when the coupled system is appropriately preconditioned.

One of the more interesting aspects of the results presented here is that, when the effects of the monsoon are parametrized in the coupled model, the model reproduces the observed lag/lead ENSO–monsoon relationship. The lag/lead ENSO–monsoon relationship in these model simulations is quite robust because the relationship was not degraded even if only 35% of the monsoon anomaly was determined from NINO3 SSTAs and 65% was random. It is not clear why more sophisticated coupled GCMs cannot reproduce the observed lag/lead relationship. For example, Kirtman and Zebiak (1997)

coupled the COLA AGCM to the same ocean component used here and, in their 50-year simulation, the contemporaneous correlation is reasonable (−0.55), but the correlation with the SSTA four months after the monsoon is only −0.2 (the observed correlation at four months is −0.71). Even with SST prescribed from observations, the AGCMs fail to capture the ENSO–monsoon relationship.

The primary limitation of the experiments presented here is that the coupled model and the parametrized monsoon are too simplistic. Moreover, we have ignored the possible impact of other elements of the climate system, such as the Pan American monsoon; nevertheless, we have demonstrated how the monsoon potentially affects ENSO. Given that monsoon variability can act as a trigger mechanism for ENSO and enhance ENSO variability, these results indicate that predicting ENSO accurately requires comprehensive coupled GCMs that correctly capture the relationship between the monsoon and ENSO.

Acknowledgements

This work benefited from discussions with V. Krishnamurthy and M. Fennessy. Figures 1(a) and (b) were provided by M. Fennessy and Fig. 2 was provided by V. Krishnamurthy. This work was supported under the National Oceanic and Atmospheric Administration grant NA26-GP0149 and the National Science Foundation (USA) grant ATM-93021354.

References

Bamzai, A. S. and Shukla, J. 1999 Relation between Eurasian snow cover, snow depth and the Indian summer monsoon: An observational study. *J. Climate*, **12,** 3117–3132

Barnett, T. P., Dumenil, L., Schlese, U., Roeckner, E. and Latif, M. 1991 'The Asian snow cover–monsoon–ENSO connection'. Pp. 191–225 in *Teleconnections linking worldwide climate anomalies*. Eds. M. H. Glantz, R. W. Katz and N. Nicholls. Cambridge University Press

Bavadekar, S. N. and Mooley, D. A. 1981 'Use of the equation of continuity of water vapor for computational average precipitation over peninsular India during the summer monsoon'. Pp. 261–268 in *Monsoon dynamics*. Eds. J. Lighthill and R. P. Pearce. Cambridge University Press

Bjerknes, J. 1969 Atmospheric teleconnections from the equatorial Pacific. *Mon. Weather Rev.*, **97,** 163–172

Chen, Y.-Q., Battisti, D. S., Palmer, T. N., Barsugli, J. and Sarachik, E. S. 1997 A study of the predictability of tropical Pacific SST in a coupled atmosphere–ocean model using singular vector analysis: The role of the annual cycle and the ENSO cycle. *Mon. Weather Rev.*, **125,** 831–845

Chung, C. and Nigam, S. 1999 Asian summer monsoon–ENSO feedback on the Cane–Zebiak model ENSO. *J. Climate*, **12,** 2787–2807

Devore, J. L. 1982 *Probability and statistics for engineering and the sciences.* Book/Cole

DeWitt, D. G. 1996 'The effect of the cumulus convection on the climate of the COLA general circulation model'. COLA Technical Report 27 (Available from COLA, 4041 Powder Mill Road, Suite 302, Calverton, MD 20705, USA)

Fennessy, M. J., Kinter III, J. L., Kirtman, B. P., Marx, L., Nigam, S., Schneider, E., Shukla, J., Straus, D., Vernekar, A., Xue, Y. and Zhou, J. 1994 The simulated Indian monsoon: A GCM sensitivity study. *J. Climate*, **7,** 33–43

Gill, A. E. 1980 Some simple solutions for the heat induced tropical circulations. *Q. J. R. Meteorol. Soc.*, **106,** 447–462

Goswami, B. N. and Shukla, J. 1991 Predictability of a coupled ocean–atmosphere model. *J. Climate*, **4,** 1–22

Goswami, B. N., Krishnamurthy, V. and Annamalai, H. 1999 A broad-scale circulation index for the interannual variability of the Indian summer monsoon. *Q. J. R. Meteorol. Soc.*, **125,** 611–633

Hahn, D. G. and Shukla, J. 1976 An apparent relationship between Eurasian snow cover and Indian monsoon rainfall. *J. Atmos. Sci.*, **33,** 2461–2462

Harshvardhan, Davis, R., Randall, D. A. and Corsetti, T. G. 1987 A fast radiation parameterization for general circulation models. *J. Geophys. Res.*, **92,** 1009–1016

Jenkins, G. M. and Watts, D. G. 1968 *Spectral analysis and its applications*. Holden-Day

Kaplan, A., Kushnir, Y., Cane, M. and Blumenthal, M. B. 1997 Reduced space optimal analysis for historical data sets: 136 years of Atlantic sea surface temperatures. *J. Geophys. Res.*, **102,** 27835–27860

Kinter III, J. L., Shukla, J., Marx, L. and Schneider, E. K. 1988 A simulation of winter and summer circulations with the NMC global spectral model. *J. Atmos. Sci.*, **45,** 2468–2522

Kinter III, J. L., DeWitt, D. G., Dirmeyer, P. A., Fennessy, M. J., Kirtman, B. P., Marx, L., Schneider, E. K., Shukla, J. and Straus, D. 1997 'The COLA atmosphere–biosphere general circulation model. Volume 1: Formulation'. COLA Technical Report 51 (Available from COLA, 4041 Powder Mill Road, Suite 302, Calverton, MD 20705, USA)

Kirtman, B. P. 1997 Oceanic Rossby wave dynamics and the ENSO period in a coupled model. *J. Climate*, **10,** 1690–1704

Kirtman, B. P. and DeWitt, D. G. 1997 Comparison of atmospheric model wind stress with three different convective parameterizations: sensitivity of tropical ocean model simulations. *Mon. Weather Rev.*, **125,** 1231–1250

Kirtman, B. P. and Schopf, P. S. 1998 Decadal variability in ENSO prediction and predictability. *J. Climate*, **11,** 2804–2822

Kirtman, B. P. and Zebiak, S. E. 1997 ENSO simulation and prediction with a hybrid coupled model. *Mon. Weather Rev.*, **125,** 2620–2641

Kirtman, B. P., Vernekar, A. D., DeWitt, D. G. and Zhou, J. 1993 Impact of orographic gravity wave drag on extended range forecasts with the COLA-GCM. *Atmosfera*, **6,** 3–24

Kirtman, B. P., Shukla, J., Huang, B., Zhu, Z. and Schneider, E. K. 1997 Multiseasonal prediction with a coupled tropical ocean global atmosphere system. *Mon. Weather Rev.*, **125,** 789–808

Lacis, A. A. and Hansen, J. E. 1974 A parameterization for the absorption of solar radiation in the earth's atmosphere. *J. Atmos. Sci.*, **31,** 118–133

Mellor, G. L. and Yamada, T. 1982 Development of a turbulence closure model for geophysical fluid problems. *Rev. Geophys. Space Phys.*, **20,** 851–875

Miyakoda, K. and Sirutis, J. 1977 Comparative integrations of global spectral models with various parameterized processes of sub-grid scale vertical transports. *Beitr. Phys. Atmos.*, **50,** 445–480

Mooley, D. A. and Parthasarthy, B. 1983 Indian summer monsoon rainfall and the east equatorial Pacific sea surface temperature. *Atmos.–Ocean*, **22,** 23–25

Moorthi, S. and Suarez, M. J. 1992 Relaxed Arakawa–Schubert: A parameterization of moist convection for general circulation models. *Mon. Weather Rev.*, **120,** 978–1002

Moore, A. M. and Kleeman, R. 1997 The singular vectors of a coupled ocean–atmosphere model of ENSO. I: Thermodynamics, energetics and error growth. *Q. J. R. Meteorol. Soc.*, **123,** 953–981

Nigam, S. 1994 On the dynamical basis for the Asian summer monsoon rainfall–El Niño relationship. *J. Climate*, **7,** 1750–1771

Parker, D. E., Jackson, M. and Horton, E. B. 1995 'The GISST sea surface temperature and sea ice climatology'. Hadley Centre Climate Research Technical Note 63. (Available from the Hadley Centre, Meteorological Office, London Road, Bracknell, Berkshire RG12 2SY, UK)

Parthasarthy, B., Rupa Kumar, K. and Munot, A. A. 1993 Homogeneous Indian monsoon rainfall: variability and prediction. *Proc. Indian Acad. Sci.*, **102,** 121–155

Rasmusson, E. and Carpenter, T. 1983 The relationship between eastern equatorial Pacific sea surface temperatures and rainfall over India and Sri Lanka. *Mon. Weather Rev.*, **111,** 517–528

Shukla, J. 1984 'Predictability of time averages. Part II: The influence of boundary forcing'. Pp. 115–206 in *Problems and prospects in long and medium range weather forecasting*, Eds. D. M. Burridge and E. Kallen. Springer-Verlag

Shukla, J. and Mintz, Y. 1982 Influence of land-surface evapotranspiration on the earth's climate. *Science*, **214,** 1498–1501

Shukla, J. and Paolino, D. A. 1983 The southern oscillation and long range forecasting of the summer monsoon rainfall over India. *Mon. Weather Rev.*, **111,** 1830–1837

Sikka, D. R. 1980 Some aspects of the large-scale fluctuations of summer monsoon rainfall over India in relation to fluctuations in the planetary and regional scale circulation parameters. *Proc. Indian Acad. Sci. (Earth and Planetary Science)*, **89,** 179–195

Sperber, K. R. and Palmer, T. N. 1996 Interannual tropical rainfall variability in general circulation model simulations associated with the atmospheric model intercomparison project. *J. Climate*, **9,** 2727–2750

Vernekar, A. D., Zhou, J. and Shukla, J. 1995 The effect of Eurasian snow cover on the Indian monsoon. *J. Climate*, **8,** 248–266

Wainer, I. and Webster, P. J. 1996 Monsoon/El Niño–Southern Oscillation relationships in a simple coupled ocean–atmosphere model. *J. Geophys. Res.*, **101,** 25599–25614

Walker, G. T. 1924 Correlations in seasonal variations of weather. *Mem. India Meteorol. Dept.*, **24,** 333–345

Webster, P. J. and Yang, S. 1992 Monsoon and ENSO: Selectively interactive systems. *Q. J. R. Meteorol. Soc.*, **118,** 877–926

Webster, P. J., Palmer, T. N., Yanai, M., Shukla, J., Magana, V., Yasunari, T. and Tomas, R. 1998 The monsoon: processes and prediction. *J. Geophys. Res.*, **105,** 14451–14510

Xie, P. and Arkin, P. A. 1996 Analysis of global monthly precipitation using gauge observations, satellite estimates and numerical model predictions. *J. Climate*, **9,** 840–858

Xue, Y., Sellers, P. J., Kinter III, J. L. and Shukla, J. 1991 A simple biosphere model for global climate studies. *J. Climate*, **4,** 345–364

Xue, Y., Cane, M. A. and Zebiak, S. E. 1997 Predictability of a coupled model of ENSO using singular vector analysis. Part I: Optimal growth in seasonal background and ENSO cycles. *Mon. Weather Rev.*, **125,** 2043–2056

Yasunari, T. 1990 Impact of Indian monsoon on the coupled atmosphere/ocean system in the tropical Pacific. *Meteorol. Atmos. Phys.*, **44,** 29–41

Yasunari, T. and Seki, Y. 1992 Role of the Asian monsoon on the interannual variability of the global climate system. *J. Meteorol. Soc. Japan*, **70,** 177–188

Zebiak, S. E. and Cane, M. A. 1987 A model of El Niño and the Southern Oscillation. *Mon. Weather Rev.*, **115,** 2262–2278